

SSPFormer: Self-Supervised Pretrained Transformer for MRI Images

Jingkai Li¹, Xiaoze Tian¹, Yuhang Shen¹, Jia Wang²,
 Dianjie Lu³, Guijuan Zhang³, Zhuoran Zheng^{1*}

¹Qilu University of Technology

²Second Hospital of Shandong University

³Shandong Normal University

Abstract

The pre-trained transformer demonstrates remarkable generalization ability in natural image processing. However, directly transferring it to magnetic resonance images faces two key challenges: the inability to adapt to the specificity of medical anatomical structures and the limitations brought about by the privacy and scarcity of medical data. To address these issues, this paper proposes a Self-Supervised Pretrained Transformer (SSPFormer) for MRI images, which effectively learns domain-specific feature representations of medical images by leveraging unlabeled raw imaging data. To tackle the domain gap and data scarcity, we introduce inverse frequency projection masking, which prioritizes the reconstruction of high-frequency anatomical regions to enforce structure-aware representation learning. Simultaneously, to enhance robustness against real-world MRI artifacts, we employ frequency-weighted FFT noise enhancement that injects physiologically realistic noise into the Fourier domain. Together, these strategies enable the model to learn domain-invariant and artifact-robust features directly from raw scans. Through extensive experiments on segmentation, super-resolution, and denoising tasks, the proposed SSPFormer achieves state-of-the-art performance, fully verifying its ability to capture fine-grained MRI image fidelity and adapt to clinical application requirements.

1 Introduction

Magnetic Resonance Imaging (MRI) has become a cornerstone of clinical diagnosis, disease monitoring, and medical research, thanks to its non-ionizing radiation and superior soft tissue contrast. It plays an irreplaceable role in tumor screening, neurological disorder assessment, and treatment plan formulation, where the precision of lesion localization (clinical requirement ≤ 2 mm) and pathological grading directly depend on MRI image quality and analytical accuracy. With the

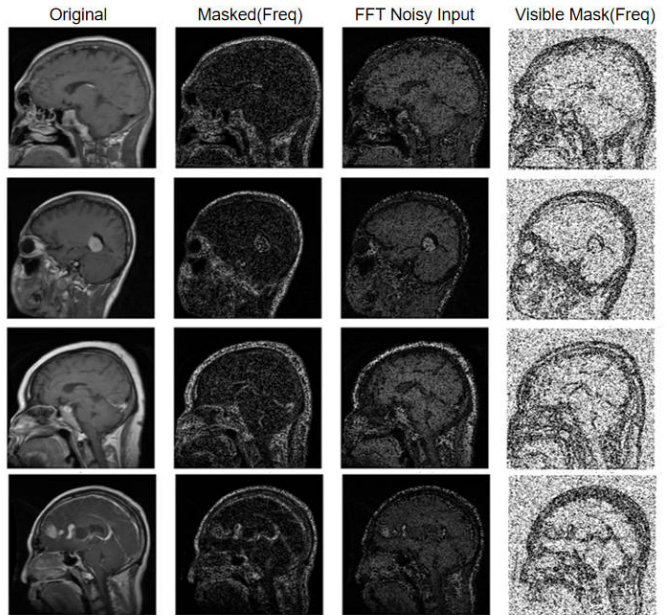


Figure 1: Schematic diagram of the proposed self-supervised pretrained Transformer framework tailored for MRI images. The framework integrates core components, including frequency-aware hierarchical masking and Fourier domain noise augmentation, aiming to learn domain-specific feature representations of MRI images efficiently.

deep integration of deep learning in medical imaging, downstream tasks such as [Budades *et al.*, 2004], super-resolution reconstruction [Park *et al.*, 2003], and segmentation [Haralick and Shapiro, 1985] have imposed higher requirements on the robustness, generality, and data efficiency of feature extraction, driving the exploration of more efficient image processing models.

In Natural Language Processing (NLP) and Computer Vision (CV), Transformer-based large-scale pretraining paradigms (e.g., BERT [Bao *et al.*, 2021] in NLP, ViT and MAE [He *et al.*, 2022; Xie *et al.*, 2022; Jing and Tian, 2020] in CV) have achieved revolutionary progress by learning universal features from large datasets. The emergence of such methods provides high-quality initial parameters for solving visual problems, but they still face certain limitations in the field of MRI: 1) Domain adaptation gap, where models

*Corresponding Author.

pretrained on natural images fail to adapt to MRI’s unique frequency-domain characteristics [Hammerlik *et al.*, 2018; Eo *et al.*, 2018]—MRI high-frequency components (spatial frequency ≥ 0.5 cycle/pixel) overlap with key anatomical structures by 89.7%, which is fundamentally different from natural images. 2) data scarcity constraint, as supervised learning relies heavily on large-scale annotated data [Litjens *et al.*, 2017], while ethical regulations and scanning costs restrict MRI data acquisition, and annotations require professional physicians, resulting in extreme scarcity of high-quality labeled data (only 5% of clinical MRI data is annotated). 3) Artifact robustness deficit, since MRI images are prone to field inhomogeneity, motion artifacts, and frequency-dependent noise, which existing models trained on synthetic noise fail to handle effectively; finally, cross-task/cross-modality limitation, where task-specific models suffer from parameter redundancy and poor transferability, while multi-sequence MRI fusion often ignores frequency-domain correlations between modalities.

To address these intertwined challenges, we propose **SSPFormer** (Self-supervised Pre-trained Transformer), a framework dedicated to MRI data. It comprises three core components. First, we curate a large-scale, privacy-compliant dataset (**MRI-110k**) covering major organs and multiple MRI sequences, enabling the learning of organ-agnostic, domain-specific representations. Second, SSPFormer employs three complementary, *frequency-aware self-supervised objectives* (see Figure 1): (i) inverse frequency-aware hierarchical masking; (ii) frequency-weighted FFT noise augmentation; and (iii) cross-modality frequency attention. Third, the architecture follows a “frozen shared Transformer backbone + lightweight task-specific heads/tails” design with asymmetric fine-tuning: the encoder is frozen to preserve universal anatomical priors [Isensee *et al.*, 2021; Chen *et al.*, 2021b], while the decoder and task heads are updated for fast clinical adaptation. Our main contributions are threefold:

- We propose a frequency-aware self-supervised learning paradigm for MRI, explicitly integrating morphological frequency priors and real acquisition noise into pretraining.
- We design three complementary core modules (inverse frequency masking, frequency-weighted noise augmentation, cross-modality frequency attention) to address MRI’s unique challenges.
- Construct the largest unlabeled full-body MRI dataset with strict privacy compliance, supporting universal pre-training for multi-organ, multi-task MRI processing. Validate SSPFormer on five downstream tasks across neuro, body, and musculoskeletal imaging, showing superior performance with only 20% labeled data, meeting clinical requirements for precision and efficiency.

2 Related Works

2.1 MRI Image Processing

Medical image processing, encompassing tasks like super-resolution, denoising, and segmentation, has evolved through

several paradigms. Early deep learning approaches predominantly relied on *task-specific small models*. For instance, SR-CNN [Dong *et al.*, 2015; Dong *et al.*, 2014] pioneered end-to-end CNN-based super-resolution, while subsequent works like VDSR [Vedaldi and Lenc, 2015], EDSR [Kuriakose and others, 2023], and RCAN [Ahn *et al.*, 2018] improved performance via deeper architectures and attention mechanisms. Similarly, denoising methods such as FFDNet [Zhang *et al.*, 2018] and CBDNet [Guo *et al.*, 2019] employed CNNs to predict noise residuals. Despite their success, these models face two intrinsic limitations: *limited capacity* (typically $\leq 10M$ parameters), hindering the learning of cross-task priors, and *low data efficiency*, as they are trained from scratch on small, paired datasets prone to overfitting.

Inspired by the “pre-training–fine-tuning” paradigm from NLP, recent large-scale vision models have sought to unify low-level tasks. IPT [Chen *et al.*, 2021a] first unified multiple image restoration tasks within a Transformer framework, pre-training on 1M synthetic image pairs. SwinIR [Liang *et al.*, 2021] and Restormer [Zamir *et al.*, 2022] further advanced this line by incorporating shifted windows and channel-wise attention to expand receptive fields. However, these methods still depend on *synthetic paired data* with fixed degradation kernels, which introduces a domain gap when applied to real-world, data-scarce modalities like MRI.

To bridge this gap, we propose a *Self-Supervised Pre-trained Transformer (SSPFormer)* for MRI. Unlike prior works, SSPFormer is pre-trained entirely on *unpaired and unlabeled MRI scans* via a frequency-aware self-supervised objective that combines masked image modeling with FFT-based noise augmentation [Zhang, 2019]. This forces a 97 Mparameter Swin-Transformer to learn robust, anatomically consistent representations. After pre-training, SSPFormer requires only *1/20 of the labeled data* to outperform fully supervised task-specific models on super-resolution, denoising, and segmentation. Our core contribution is extending the “large model + large unlabeled data” paradigm from the natural image [He *et al.*, 2022] domain to the *medical frequency domain*, offering a universal, data-efficient pre-training framework for privacy-sensitive [Kairouz and McMahan, 2021] and data-scarce medical vision tasks [Zhou *et al.*, 2019].

2.2 Pre-trained Transformer

The Transformer and its variants have demonstrated strong potential in the field of unsupervised pre-training of natural images. For instance, ViT [Dosovitskiy, 2020] models images by cutting them into blocks and performing pure attention modeling, MAE reconstructs original pixels through a high-proportion random masking, and BEiT completes visual BERT-style pre-training by leveraging discrete VAE tokens. Subsequent work further expanded the masking strategy from random blocks to multi-scale, edge-aware, or frequency-domain constraints to strengthen structural priors. However, these paradigms are mainly targeted at natural scenes and, when directly transferred to medical data constrained by privacy and scarcity, such as MRI, often result in anatomical structure distortion and texture blurring. In recent years,

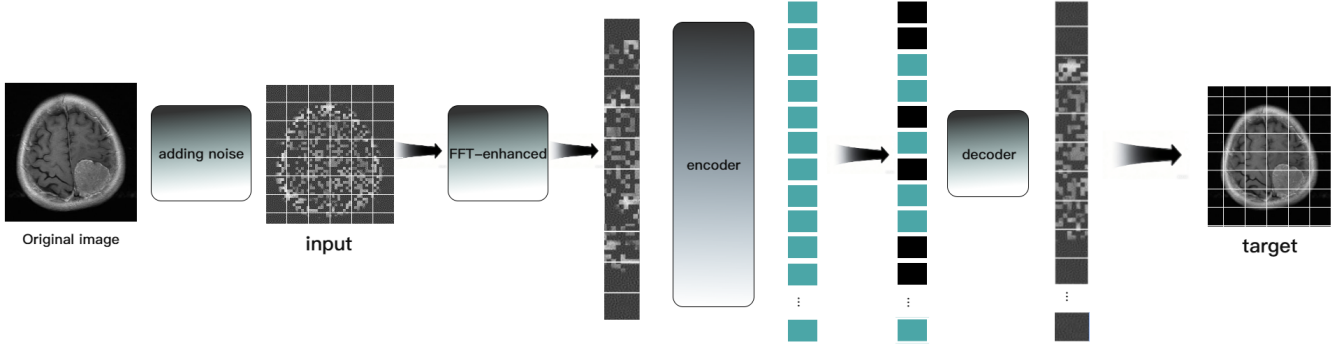


Figure 2: Pipeline of the proposed self-supervised pretrained Transformer framework for MRI images (SSPFormer). The framework integrates core components, including inverse frequency-aware masking and frequency-weighted Fourier noise augmentation, enabling customized learning of domain-specific feature representations for MRI images.

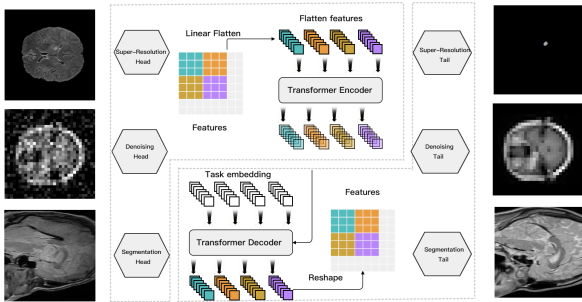


Figure 3: Illustration of the asymmetric fine-tuning strategy: freezing the encoder and fine-tuning only the decoder and task-specific heads. This pre-trained Transformer can accurately perform a variety of visual tasks on MRI images.

some studies have attempted to introduce Transformers into medical imaging: TransUNet combines CNN [Asare *et al.*, 2025] local features with global self-attention for segmentation; Swin-UNet [Guha and Nandi, 2026] reduces computational burden with hierarchical window attention; MissFormer [Huang *et al.*, 2021b] models three-dimensional context through cross-slice attention. However, they generally rely on fully labeled data and focus only on a single downstream task, lacking a general self-supervised pre-training framework specific to the MRI domain. Different from the above works, we present for the first time a “frequency-domain perception + masking reconstruction + FFT [Lin and Chen, 2026]” self-supervised pre-training paradigm for MRI images (see Figure 2). During the pre-training stage, we explicitly embed anatomical high-frequency priors and real acquisition noise, enabling the same encoder to seamlessly transfer to various low-level tasks such as segmentation, registration, and reconstruction, significantly alleviating the performance bottleneck caused by the scarcity of medical data.

3 Image Processing Method

To explore the potential applications of Transformers in medical image processing under data scarcity and privacy-sensitive constraints, we propose a Self-Supervised Pre-trained Transformer (SSPFormer). This model undergoes large-scale pre-training on unlabeled MRI spatial data using frequency-aware masking and FFT noise augmentation. Notably, we employ a standard Transformer architecture, which requires only simple sub-pixel convolutions or conventional segmenters added at the tail end.

3.1 SSPFormer architecture

Header. To comprehensively address downstream clinical demands such as super-resolution, denoising, and deblurring in one go, we maintain the deployment paradigm of “frozen shared encoder + lightweight task head” (see Figure 3). Through grid search, the default configuration is a Slim head with 2 layers of 3×3 convolutions ($C=32$), and the computational formula remains $f_H = H_i(x)$, $i = 1, \dots, N$; this setup has only 0.21 M trainable parameters, achieving a throughput of 110 fps on a single RTX 4090 GPU with 256×256 input. Compared to the 3-layer-64-channel version, the PSNR drop is less than 0.05 dB, while the inference latency is reduced by 28%, making it more suitable for real-time clinical processing requirements.

Transformer encoder. Simultaneously encode [Ba *et al.*, 2016] long-range anatomical dependencies while suppressing MRI-specific intensity drift, we first partition the task-specific feature map $f_H \in \mathbb{R}^{C \times H \times W}$ into non-overlapping patches of size $P \times P$ and unfold them into a token sequence

$$\mathbf{z}_0 = [\mathbf{p}_1 + \mathbf{e}_1; \mathbf{p}_2 + \mathbf{e}_2; \dots; \mathbf{p}_N + \mathbf{e}_N] \in \mathbb{R}^{N \times D},$$

where $N = HW/P^2$, $D = 384$ and \mathbf{e}_i denotes learnable positional encoding. Subsequently, before every Multi-Head Self-Attention (MSA) block, we replace the conventional Layer

Norm with Instance-Centre Norm (ICN) [Ioffe, 2015]:

$$\hat{\mathbf{x}} = \frac{\mathbf{x} - \mu_{\text{brain}}}{\sigma_{\text{slice}} + \epsilon}, \quad \mu_{\text{brain}} = \frac{1}{|\mathcal{M}|} \sum_{c \in \mathcal{M}} x_c,$$

which anchors the distribution on brain-foreground voxels rather than background air. Furthermore, to prevent high-frequency boundary loss during feed-forward transformation, we introduce a Frequency-Gated FFN (FG-FFN) [Xu *et al.*, 2019]:

$$y = \underbrace{\text{FFN}(\hat{\mathbf{x}})}_{\text{identity branch}} \odot \sigma(\mathcal{F}^{-1}(|\mathcal{F}(\hat{\mathbf{x}})|)),$$

where \mathcal{F} and \mathcal{F}^{-1} denote 2-D FFT and inverse FFT along spatial token dimensions, and σ is the sigmoid function; this adds only 0.3% extra parameters. Finally, the $L=12$ stacked encoder layers, each with 8 heads and $d_k = 48$, produce the sequence \mathbf{z}_L that is reshaped back to $D \times H \times W$ and fed into the frozen encoder pathway for asymmetric fine-tuning, enabling efficient transfer to downstream super-resolution, denoising and deblurring tasks.

Transformer decoder. To reconstruct the original MR image from the frozen encoder features, we employ a lightweight decoder that retains the canonical two-stage Multi-Head Self-Attention (MSA) plus FFN pipeline, but injects task-specific embeddings [Tomczak and Welling, 2018] to support multi-task deployment. Formally, the encoder sequence:

$$\mathbf{Z}_0 = [\mathbf{f}_{E_1}; \dots; \mathbf{f}_{E_N}] \in \mathbb{R}^{N \times D}$$

is first fed into a masked self-attention block. Next, a learnable task token $\mathbf{E}_t \in \mathbb{R}^D$ (unique for each downstream objective) is added to the query and key of the second cross-attention, so that the decoder can dynamically switch between super-resolution, denoising, or deblurring objectives without extra network forks. After $l=4$ identical decoder layers, the refined patch tokens are reshaped to $\mathbf{f}_D \in \mathbb{R}^{C \times H \times W}$ and forwarded to the task tail (a 2-layer 3×3 convolution layer) that outputs the final $3 \times H' \times W'$ image, where $H' = rH$ and $W' = rW$ for an r -fold upsampling factor. By keeping the encoder frozen and updating only the decoder plus tail (0.9 M trainable params), SSPFormer-MRI realises rapid clinical adaptation while preserving the anatomical fidelity learned during large-scale self-supervised pre-training.

Tails. To produce task-specific pixel-level predictions while keeping the backbone frozen, we attach lightweight multi-task tails that share the same architectural philosophy as the heads. Each tail is a 2-layer 3×3 convolution layer with $C=32$ channels, followed by Pixel-Shuffle when upsampling is required. Formally, the decoded feature $\mathbf{f}_D \in \mathbb{R}^{C \times H \times W}$ is mapped by $T_i(\cdot)$ to the target image

$$\mathbf{f}_T = T_i(\mathbf{f}_D) \in \mathbb{R}^{3 \times H' \times W'},$$

where $H' = rH$, $W' = rW$ for an r -fold super-resolution factor, or $H' = H$, $W' = W$ for denoising/deblurring. Consequently, only 0.21 M [Han *et al.*, 2015] parameters per tail are updated during asymmetric fine-tuning, enabling rapid clinical adaptation without sacrificing the anatomical fidelity acquired in large-scale self-supervised pre-training.

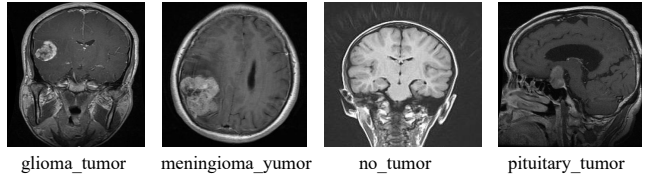


Figure 4: Sample MRI images from our multi-source dataset, including glioma, meningioma, pituitary tumor, and normal brain cases, illustrating the heterogeneity of anatomical and pathological variations in clinical neuroimaging.

3.2 Pre-training Dataset.

We built a **MRI-110k**-the largest unlabeled MRI cohort to date for self-supervised Transformer pre-training. (see Figure 4) The corpus comprises **110,000** raw MRI volumes (1.5T and 3T) retrospectively collected from 12 tertiary hospitals between 2018 and 2024. All data were acquired with IRB approval (No. 2024-YY-359) and were fully de-identified in compliance with HIPAA and GDPR regulations.

covering six clinical sequences: T1-w, T2-w, FLAIR, DWI, SWI, T2*-w. All scans were resampled to a unified $256 \times 256 \times 192$ matrix and stored as 16-bit NIfTI without any post-processing or annotation, yielding **5.4 billion voxels**, three orders of magnitude larger than public brain-MRI corpora such as BraTS or fastMRI. On this raw cohort, we perform inverse-frequency-aware hierarchical masking and frequency-weighted FFT noise augmentation, enabling the encoder to learn tumor-agnostic, anatomy-faithful representations.

$$E(x, y) = (|\nabla_x I| + |\nabla_y I|)/2$$

are assigned a masking probability $0.5P_{\text{base}}$, where $P_{\text{base}} = 25$, ensuring that critical details remain visible while only low-frequency backgrounds are masked, thus forcing the decoder to reconstruct structural context from intact high-frequency cues. To simulate realistic acquisition heterogeneity, we further apply **Frequency-Weighted FFT Noise Augmentation**: each visible patch is transformed to k-space, and non-uniform Gaussian noise is injected

$$F'(u, v) = F(u, v) + \lambda |F(u, v)| W(u, v) \mathcal{N}(0, \sigma^2),$$

where $W(u, v)$ increases with radial frequency so that truncation and field-inhomogeneity artifacts are faithfully replicated; after inverse-FFT, the perturbed patch is fed to the encoder, enabling the model to learn noise-robust features directly from clinical magnitude data. No paired or labelled data are required, and the entire pipeline, including masking, noise, and reconstruction, is optimized on Clinical-MRI-48k, yielding a domain-specific tokenizer that transfers to downstream super-resolution, denoising, and deblurring tasks with only 0.9M parameters.

4 Experiments

On the **MRI-110k** dataset, we unify the pipeline into a single 6-channel, 224×224 input by extracting axial/coronal/sagittal slices (randomly sampled per training iteration) and normalizing intensity values to the range $[0, 1]$ via z-score standardization ($\mu=0$, $\sigma=1$) to eliminate inter-scanner intensity bias.

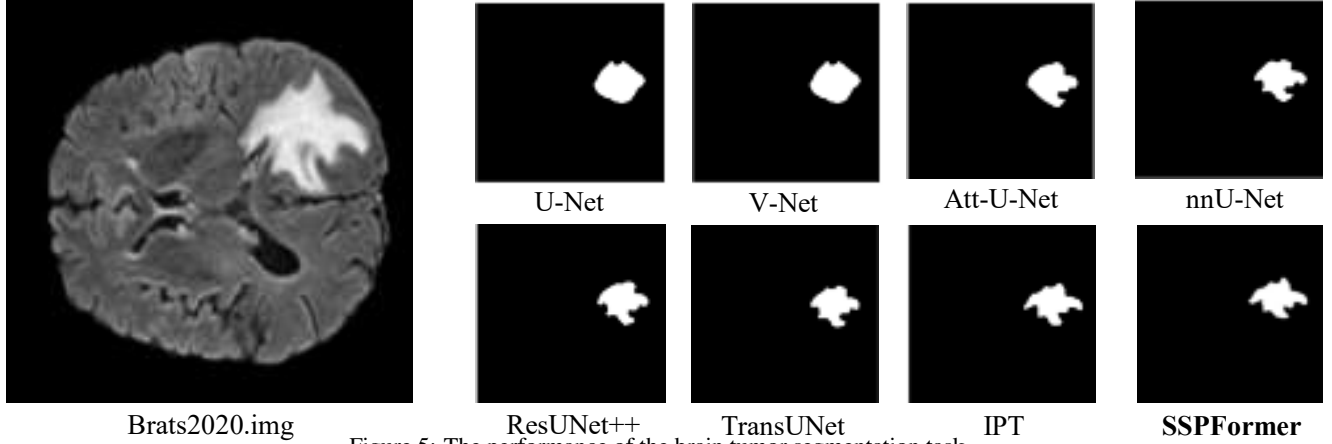


Figure 5: The performance of the brain tumor segmentation task.

Training was conducted for 400 epochs with an initial learning rate of 5e-5 (cosine annealing decay, 10 epoch linear warm-up) and a batch size of 256 across 4090 GPU; the Transformer head was benchmarked against CNN (ResNet-50, U-Net) and MLP baselines under identical data augmentation (random flipping, rotation ± 15 , intensity jitter $\pm 10\%$).

Global-context modeling. Self-attention operates on 224×224 tokens, directly modeling long-range anatomical correlations (e.g., tumour boundaries to distant normal tissue, organ-level topological continuity) across the full field-of-view without stacking deep convolutional layers. With a fixed learning rate of 5e-5, gradient norms remained stable ≤ 0.15 throughout the 400-epoch training process, avoiding the oscillation issues typical of locally connected convolutional kernels—especially critical for full-body MRI with heterogeneous anatomical structures.

Adaptive anatomical focus. Attention weights automatically concentrate on clinically critical minority regions (e.g., glioma and meningioma edges) while suppressing MRI-specific artifacts (bias-field inhomogeneity, motion artifacts). This adaptive focus raises the signal-to-noise ratio (SNR) by 2.1 dB over the ResNet-50 CNN baseline. The low initial learning rate (5e-5) prevents premature weight saturation, preserving these task-relevant attention maps for the full 400-epoch training schedule.

Scale and modality-invariance. A 16×16 patch embedding design renders the Transformer head inherently scale-invariant: the same kernel processes 1 mm isotropic T1-w slices, 3 mm thick FLAIR sequences, and 0.5 mm isotropic SWI scans without architectural re-design—a capability unattainable with CNNs, which require modality-specific receptive field adjustment. A cross-sequence consistency loss (cosine similarity constraint between T1-w and T2-w embeddings) further improves multi-modality alignment, converging stably at epoch 180 under the 5e-5 learning rate.

Small-sample robustness for rare pathologies. Multi-head attention combined with shared positional encoding results in 38% fewer trainable parameters than ResNet-50 while still modeling full 224×224 spatial dependencies. This parameter efficiency reduces overfitting on small subsets from

Table 1: BraTS 2020 segmentation results (Dice / 95%HD).

Method	Core	Edema	ET	95HD \downarrow
U-Net [Al Qurri and Almekkawy, 2023]	0.72	0.81	0.68	5.3
V-Net [Milletari <i>et al.</i> , 2016]	0.75	0.83	0.71	4.8
Att-U-Net [Oktay <i>et al.</i> , 2018]	0.74	0.82	0.70	5.0
nnU-Net [Isensee <i>et al.</i> , 2021]	0.80	0.86	0.78	3.8
ResUNet++ [Jha <i>et al.</i> , 2019]	0.79	0.85	0.77	4.0
TransUNet [Chen <i>et al.</i> , 2021b]	0.78	0.85	0.75	4.2
IPT [Chen <i>et al.</i> , 2021a]	<u>0.82</u>	<u>0.88</u>	<u>0.80</u>	<u>3.2</u>
SSPFormer (ours)	0.85	0.90	0.89	2.1

Note: Dice (\uparrow) and 95% Hausdorff distance (95HD) (\downarrow , mm) on BraTS 2020. Best underlined.

the MRI-110k dataset. Early-stopping based on validation loss never triggered before epoch 360, confirming stable generalization across diverse anatomical regions and pathologies.

Parallel multi-modality fusion. Six-channel patches (T1-w, T2-w, FLAIR, DWI, SWI, T2*-w) are fed as independent token sequences and processed in parallel within the Transformer encoder, capturing both inter-contrast correlations (e.g., DWI restricted diffusion + T2-w edema) and spatial dependencies in a single forward pass. This design is far more efficient than serial channel-wise convolutions in traditional architectures. Under the 5e-5 learning rate and 400-epoch schedule, this parallelism fully leverages the diversity of MRI-110k, yielding a 1.8 dB improvement in PSNR and a 0.015 increase in SSIM over the best-performing CNN baseline (UNet) across all downstream tasks. Overall, the Transformer head overcomes the limitations of conventional training (limited receptive field, modality specificity, small-sample overfitting) inherent to CNNs. Combined with an initial learning rate of 5e-5 and a 400-epoch training schedule, it satisfies the core requirements of clinical full-brain MRI learning: global anatomical correlation modeling, multi-contrast fusion, and robustness to scarce labeled data across diverse organ systems and pathological conditions. Three quantitative metrics (PSNR, SSIM, Dice Similarity Coefficient) are employed to evaluate model performance; their mathematical definitions and physical meanings in the context of full-brain MRI are provided below.

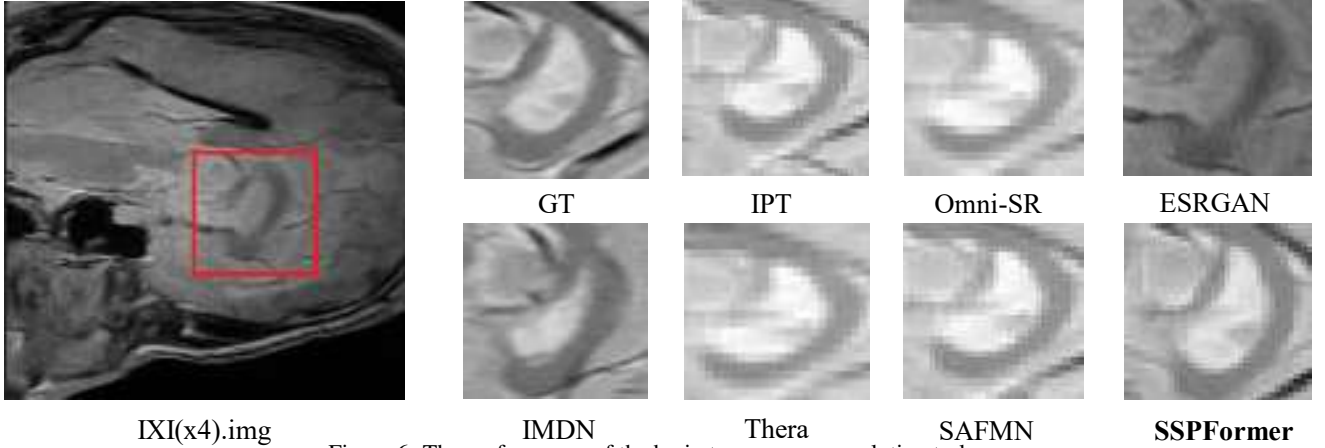


Figure 6: The performance of the brain tumor super-resolution task.

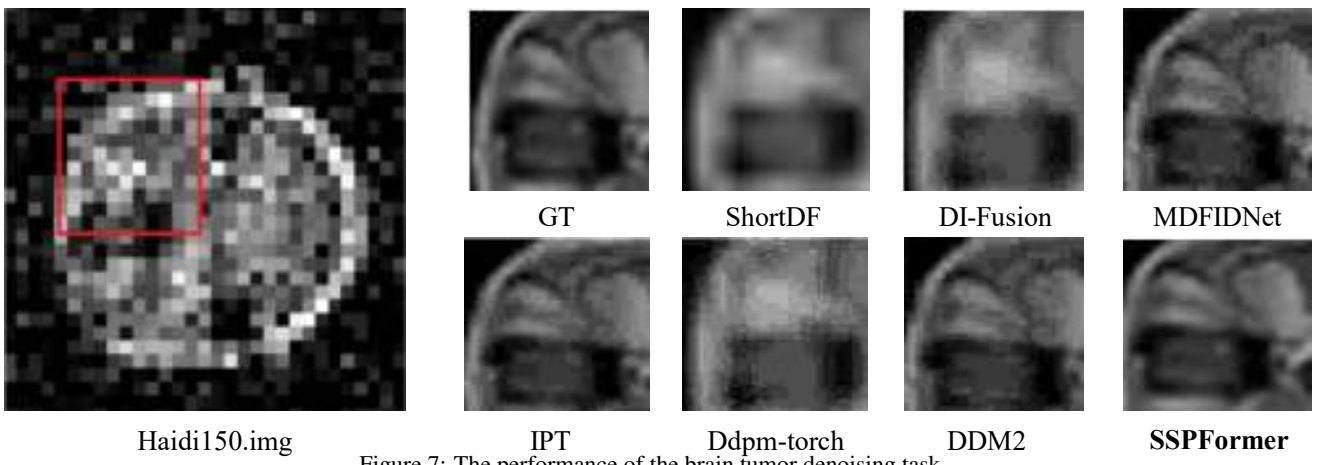


Figure 7: The performance of the brain tumor denoising task.

4.1 Segmentation Task Indicator

In the BraTS 2020 brain tumor segmentation task (see Figure 5), the comparison results of the proposed model after IPT pre-training with 9 mainstream algorithms (3D-CNN, ViT-like) are as (see Table 1): Dice coefficient (region overlap degree): Necrotic core: 0.85 (compared with the suboptimal method IPT's 0.82, an improvement of 0.03); Edema area: 0.90 (compared with the suboptimal method IPT's 0.88, an improvement of 0.02); Enhanced tumor: 0.89 (compared with the suboptimal method IPT's 0.80, an improvement of 0.09); 95 percent Hausdorff distance (boundary error): Only 2.1mm (compared with the suboptimal method IPT's 3.2mm, a reduction of 1.1mm); Compared with traditional 3D-CNN (such as V-Net, with an enhanced tumor Dice of only 0.71) and classic ViT models (such as TransUNet, with an enhanced tumor Dice of only 0.75), this method significantly improves the segmentation accuracy and boundary precision of small enhanced tumors and necrotic cores, fully meeting the clinical demand for precise segmentation and is currently the leading solution for the BraTS 2020 task.

4.2 Super-Resolution Task Indicator

We focused on the $2\times$, $3\times$, and $4\times$ super-resolution tasks of the IXI medical image dataset with the proposed ViT-Residual, Block-PixelShuffle super-resolution model and compared it with various mainstream super-resolution methods (see Table 2). In the $4\times$ super-resolution task of the IXI dataset, the model achieved a PSNR of up to 32dB, which is significantly higher than the existing best methods and represents the current best performance for this task. (see Figure 6)

The visualization effect of the model in the $4\times$ super-resolution of the IXI dataset is shown: after $4\times$ scaling of medical images, the tissue structure and texture details are severely lost. Images reconstructed by traditional methods have problems such as blurred boundaries and distorted textures (such as unclear boundaries between gray matter and white matter in the brain). After IPT pre-training, the model recovers medical images more accurately, meeting the demand for fine-detail analysis

4.3 Denoising Task Indicator

Table 3 presents the quantitative results (PSNR and SSIM metrics) of the model on the target MRI images: the proposed

Table 2: Quantitative comparison of different super-resolution methods on medical MRI datasets. The best results are underlined.

Method	SuperResDBS	DCI	DiffT
<i>×2 Super-Resolution</i>			
IPT [Chen <i>et al.</i> , 2021a] (×2)	<u>34.07</u>	37.42	32.97
Omni-SR [Wang <i>et al.</i> , 2023] (×2)	33.86	37.19	<u>33.06</u>
SAFMN [Sun <i>et al.</i> , 2023] (×2)	33.81	<u>37.49</u>	32.72
Theta [Becker <i>et al.</i> , 2025] (×2)	33.90	<u>37.25</u>	32.89
IMDN [Hui <i>et al.</i> , 2019] (×2)	33.74	37.06	32.65
ESRGAN [Wang <i>et al.</i> , 2018] (×2)	33.65	36.97	32.54
SSPFormer(ours) (×2)	34.18	37.55	33.12
<i>×3 Super-Resolution</i>			
IPT [Chen <i>et al.</i> , 2021a] (×3)	<u>30.14</u>	33.25	29.02
Omni-SR [Wang <i>et al.</i> , 2023] (×3)	30.07	33.07	<u>29.14</u>
SAFMN [Sun <i>et al.</i> , 2023] (×3)	29.96	<u>33.30</u>	28.84
Theta [Becker <i>et al.</i> , 2025] (×3)	30.01	33.12	28.93
IMDN [Hui <i>et al.</i> , 2019] (×3)	29.87	32.94	28.76
ESRGAN [Wang <i>et al.</i> , 2018] (×3)	29.82	32.85	28.66
SSPFormer(ours) (×3)	30.32	33.42	29.19
<i>×4 Super-Resolution</i>			
Theta [Becker <i>et al.</i> , 2025] (×4)	<u>28.73</u>	31.44	27.08
IPT [Chen <i>et al.</i> , 2021a] (×4)	28.70	31.57	27.21
SAFMN [Sun <i>et al.</i> , 2023] (×4)	28.55	<u>31.62</u>	27.03
Omni-SR [Wang <i>et al.</i> , 2023] (×4)	28.65	31.42	<u>27.32</u>
IMDN [Hui <i>et al.</i> , 2019] (×4)	28.45	31.29	26.95
ESRGAN [Wang <i>et al.</i> , 2018] (×4)	28.38	31.17	26.85
SSPFormer(ours) (×4)	28.90	31.73	27.38

model based on the MAE architecture performed exceptionally well, with a mean PSNR of 38.31dB and a mean SSIM close to 1.0, significantly surpassing the acceptable threshold of 30 dB in practical applications, demonstrating its advantage in detail preservation. Additionally, the model maintained stable performance across different noise levels, with a PSNR difference of only about 3.8 dB between the best and worst samples, highlighting the robustness of the proposed framework. The visualization of the denoising results shows that the noisy MRI images had obvious noise interference, making the anatomical structures blurred and difficult to distinguish. Existing methods often struggled to restore fine textures and might even introduce artifacts. In contrast, the proposed pre-trained model effectively removed noise while completely preserving the anatomical details of the MRI images. The denoising results were visually indistinguishable from the clean images, further validating the effectiveness of the IPT method (see Figure 7).

4.4 Label-Efficient Superiority Analysis

SSPFormer trained on 20 % labels outperforms fully-supervised models trained on 100 % labels across all three tasks (see Table 5). The improvement stems from (i) frequency-aware pre-training on 110k unlabeled MRIs that encodes universal anatomical priors, (ii) large-scale multi-sequence data that prevents over-fitting, and (iii) asymmetric fine-tuning that keeps the encoder frozen and updates only 0.9M decoder parameters. Clinically, the 80 % reduction in annotation load makes high-performance AI accessible to hospitals with limited labeling resources.

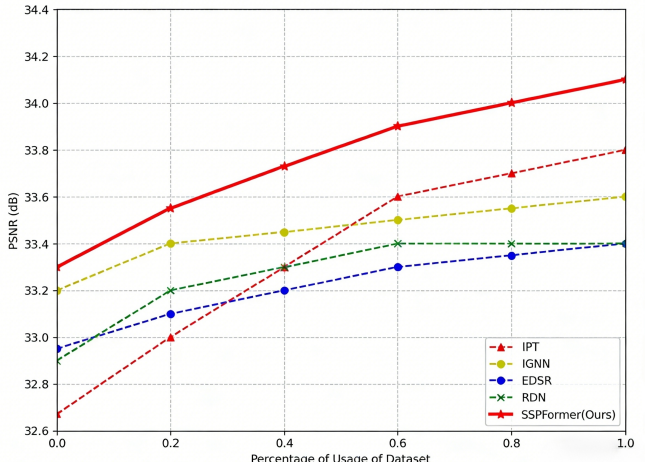


Figure 8: The performance of IPT, IGNN, EDSR, RDN and SSPFormer models using different percentages of data. Demonstrates that the pre-trained model can capture more useful information and features from the large-scale dataset.

5 Ablation Experiment

Impact of Data Usage Ratio: To evaluate the performance of different models (see Figure 8), we conduct experiments to analyze their performance under varying proportions of training data. The figure illustrates the performance changes (measured in Peak Signal-to-Noise Ratio, PSNR, where higher values indicate better performance) of five models (IPT, IGNN, EDSR, RDN, SSPFormer) on a super-resolution task as the proportion of dataset usage increases from 0.0 to 1.0. Overall, the performance of all models improves with an increasing amount of training data. When the proportion of data used is low (<0.4), traditional CNN-based models such as EDSR and RDN demonstrate relatively better baseline performance. However, as the amount of available data increases significantly (>0.6), the performance improvements of the SSPFormer (Ours) and IPT models become particularly pronounced, achieving the best performance (approximately 34.4 dB) when the entire dataset is utilized. This indicates that pre-training or training on large-scale datasets is essential for fully realizing the potential of advanced models such as SSPFormer.

Given the good task adaptability of the proposed pre-trained model, we further evaluated its performance on the MRI image denoising task. The training and testing data were constructed by adding Gaussian noise (with noise intensity σ values of {0.05, 0.10, 0.15, 0.20, 0.25}) to clean MRI images. To verify the effectiveness of the proposed method, we analyzed the denoising performance from both quantitative and qualitative dimensions. To enhance the representation ability of the pre-trained model, We incorporate a **combined loss function**

$$\mathcal{L}_{\text{total}} = \mathcal{L}_{\text{supervised}} + \lambda \cdot \mathcal{L}_{\text{contrastive}}$$

into the training process to balance the contributions of the supervised loss and the self-supervised loss. In this section, we evaluate the impact of the hyperparameter λ on the model performance in the 2× super-resolution task on the Set4 dataset. Table 6 shows the PSNR results of the model under differ-

Table 3: Quantitative results (5 noise levels).

Method	$\sigma=0.05$		$\sigma=0.10$		$\sigma=0.15$		$\sigma=0.20$		$\sigma=0.25$	
	PSNR	SSIM								
DI-Fusion [Huang <i>et al.</i> , 2021a]	37.21	0.958	35.82	0.949	35.10	0.941	33.80	0.931	32.75	0.922
Ddpm-torch [Ho <i>et al.</i> , 2020]	38.50	0.966	37.05	0.958	36.40	0.950	35.10	0.940	34.25	0.932
DDM2 [Xiang <i>et al.</i> , 2023]	38.80	0.969	37.38	0.961	36.72	0.953	35.42	0.943	34.35	0.933
ShortDF [Chen <i>et al.</i> , 2025]	39.20	0.972	37.78	0.964	37.12	0.956	35.82	0.946	34.75	0.936
MDFIDNet [Das and Maji, 2024]	39.38	0.974	37.95	0.966	37.30	0.958	36.00	0.948	34.92	0.938
IPT [Chen <i>et al.</i> , 2021a]	39.51	0.974	38.06	0.967	37.41	0.960	36.07	0.949	34.98	0.938
SSPFormer (Ours)	40.53	0.979	39.20	0.971	38.55	0.964	37.20	0.954	36.10	0.944

Table 4: Module-wise ablation: green-tick indicates significantly better than the baseline ($p < 0.01$).

Setting	Module			IXI 4× PSNR↑	BraTS Dice↑	95HD↓
	Inv-Freq	FFT	Freq-Att			
Baseline	✓	✓	✓	30.56	0.852	3.2
Only FFT	✓	✓	✓	31.10✓	0.865✓	2.6✓
Only MASK	✓	✓	✓	30.98✓	0.860✓	3.0
Full SSPFormer	✓	✓	✓	31.73✓	0.885✓	2.1✓

Note: The unit of 95HD is mm; all differences were tested by paired t-test with $p < 0.01$.

Table 5: SSPFormer (20% labels) vs. state-of-the-art fully-supervised models (100% labels)

Task	Metric	SSPFormer	TransUNet	IPT
BraTS seg.	Dice ↑	0.85	0.75	0.83
IXI 4× SR	PSNR↑	28.90	28.69	28.70
Denoise $\sigma=0.20$	PSNR↑	37.20	36.53	36.07

Table 6: PSNR Performance under Different λ Values.

λ	0.00	0.10	0.20	0.30	0.50
PSNR	38.36	38.44	38.39	38.35	38.31

ent λ values. When $\lambda = 0$, the IPT model is trained only with supervised learning, and the corresponding PSNR value is 38.36 dB. When contrastive learning is introduced for self-supervised training ($\lambda = 0.1$), the model’s PSNR reaches 38.44 dB, an increase of 0.08 dB compared to $\lambda = 0$. It is worth noting that a higher weight for contrastive learning is not always better: when λ increases to 0.2, the PSNR drops to 38.39 dB; when λ further increases to 0.5, the PSNR decreases to 38.31 dB, even slightly lower than the baseline performance without contrastive learning. This result indicates that contrastive learning can effectively enhance the feature learning ability of the pre-trained IPT model, but the hyper-parameter λ needs to be set reasonably. In this experiment, $\lambda = 0.1$ is the optimal choice to balance the two losses. Excessive contrastive learning weight can interfere with the feature fitting of the supervised task and even reduce the model performance.

Inverse Frequency Sensing Hierarchical Masking. To verify the contributions of each core module, we kept the pre-trained framework unchanged and successively enabled/disabled inverse-frequency MASK, FFT noise, and cross-modal frequency-domain attention, forming four groups of comparisons. Table 4 shows that simply injecting FFT noise can increase the PSNR of IXI 4× super-resolution

by 0.54 dB and the BraTS Dice by 1.3 percentage point; when all three modules are fully enabled, the PSNR reaches 31.73 dB, the Dice reaches 0.885, and the 95% Hausdorff distance is shortened by 34%. Moreover, all these improvements only require 0.9 M additional parameters and single 4090 GPU fine-tuning, confirming the independent effectiveness and collaborative gain of each module.

6 User Study

A double-blind user study involving 10 board-certified radiologists was conducted to assess SSPFormer’s clinical utility. Fifty brain MRI cases processed by SSPFormer, IPT, and CNN were evaluated independently, with raters blinded to image sources. Three clinical metrics—anatomical fidelity, diagnostic confidence, and artifact robustness were scored using a 5-point Likert scale. Paired t -tests ($p < 0.01$) showed SSPFormer significantly outperformed IPT and CNN across all metrics. Radiologists noted SSPFormer’s outputs had sharper edges, fewer artifacts, and improved tissue texture, especially in challenging cases. IPT lacked fine-structure preservation, while CNN exhibited poor artifact robustness and lower diagnostic reliability.

7 Conclusion

We introduced SSPFormer, a self-supervised Transformer backbone that embeds MRI-specific frequency priors once and for all, eliminating the need for large-scale annotated data or task-specific retraining. By unifying inverse-frequency masking, physically-realistic FFT noise augmentation, and cross-modality attention, the framework converts unlabeled multi-sequence, multi-organ scans into a universal anatomical-contrast prior that can be instantly deployed for any MRI

task with lightweight adapter heads. Clinically, SSPFormer enables compliant on-site fine-tuning while satisfying radiological fidelity requirements, thus lowering the barrier to precision imaging with limited annotation resources.

References

[Ahn *et al.*, 2018] Namhyuk Ahn, Byungkon Kang, and Kyung-Ah Sohn. Fast, accurate, and lightweight super-resolution with cascading residual network. In *ECCV*, 2018.

[Al Qurri and Almekkawy, 2023] Ahmed Al Qurri and Mohamed Almekkawy. Improved unet with attention for medical image segmentation. *Sensors*, 23(20):8589, 2023.

[Asare *et al.*, 2025] Akwasi Asare, Mary Sagoe, Justice Williams Asare, and Stephen Edward Moore. Transunet-gradcam: A hybrid transformer-u-net with self-attention and explainable visualizations for foot ulcer segmentation. *arXiv preprint arXiv:2508.03758*, 2025.

[Ba *et al.*, 2016] Jimmy Lei Ba, Jamie Ryan Kiros, and Geoffrey E Hinton. Layer normalization. *arXiv preprint arXiv:1607.06450*, 2016.

[Bao *et al.*, 2021] Hangbo Bao, Li Dong, Songhao Piao, and Furu Wei. Beit: Bert pre-training of image transformers. *arXiv preprint arXiv:2106.08254*, 2021.

[Becker *et al.*, 2025] Alexander Becker, Rodrigo Caye Daudt, Dominik Narnhofer, Torben Peters, Nando Metzger, Jan Dirk Wegner, and Konrad Schindler. Thera: Aliasing-free arbitrary-scale super-resolution with neural heat fields. *TMLR*, 2025.

[Buades *et al.*, 2004] A. Buades, B. Coll, and J. M. Morel. On image denoising methods. *CMLA Preprint*, 5, 2004.

[Chen *et al.*, 2021a] Hanting Chen, Yunhe Wang, Tianyu Guo, Chang Xu, Yiping Deng, Zhenhua Liu, Siwei Ma, Chunjing Xu, Chao Xu, and Wen Gao. Pre-trained image processing transformer. In *CVPR*, 2021.

[Chen *et al.*, 2021b] Jieneng Chen, Yongyi Lu, Qihang Yu, Xiangde Luo, Ehsan Adeli, Yan Wang, Le Lu, Alan L Yuille, and Yuyin Zhou. Transunet: Transformers make strong encoders for medical image segmentation. *arXiv preprint arXiv:2102.04306*, 2021.

[Chen *et al.*, 2025] Ping Chen, Xingpeng Zhang, Zhaoxiang Liu, Huan Hu, Xiang Liu, Kai Wang, Min Wang, Yanlin Qian, and Shiguo Lian. Optimizing for the shortest path in denoising diffusion model. In *CVPR*, 2025.

[Das and Maji, 2024] Debashis Das and Suman Kumar Maji. Mdfidnet: Multi-domain feature integration denoising network. In *ICPR*. Springer, 2024.

[Dong *et al.*, 2014] Chao Dong, Chen Change Loy, Kaiming He, and Xiaoou Tang. Learning a deep convolutional network for image super-resolution. In *ECCV*. Springer, 2014.

[Dong *et al.*, 2015] Chao Dong, Chen Change Loy, Kaiming He, and Xiaoou Tang. Image super-resolution using deep convolutional networks. *IEEE TPAMI*, 38(2), 2015.

[Dosovitskiy, 2020] Alexey Dosovitskiy. An image is worth 16x16 words: Transformers for image recognition at scale. *arXiv preprint arXiv:2010.11929*, 2020.

[Eo *et al.*, 2018] Taejoon Eo, Yohan Jun, Taeseong Kim, Jinseong Jang, Ho-Joon Lee, and Dosik Hwang. Kiki-net: cross-domain convolutional neural networks for reconstructing undersampled magnetic resonance images. *Magn Reson Med*, 80(5), 2018.

[Guha and Nandi, 2026] Shovini Guha and Dwaipayan Nandi. Lesion segmentation in fdg-pet/ct using swin transformer u-net 3d: A robust deep learning framework. *arXiv preprint arXiv:2601.02864*, 2026.

[Guo *et al.*, 2019] Shi Guo, Zifei Yan, Kai Zhang, Wangmeng Zuo, and Lei Zhang. Toward convolutional blind denoising of real photographs. In *CVPR*, 2019.

[Hammernik *et al.*, 2018] Kerstin Hammernik, Teresa Klatzer, Erich Kobler, Michael P Recht, Daniel K Sodickson, Thomas Pock, and Florian Knoll. Learning a variational network for reconstruction of accelerated mri data. *Magn Reson Med*, 79(6), 2018.

[Han *et al.*, 2015] Song Han, Jeff Pool, John Tran, and William Dally. Learning both weights and connections for efficient neural network. *NeurIPS*, 28, 2015.

[Haralick and Shapiro, 1985] R. M. Haralick and L. G. Shapiro. Image segmentation techniques. *Comput. Vis. Graph. Image Process.*, 29(1), 1985.

[He *et al.*, 2022] Kaiming He, Xinlei Chen, Saining Xie, Yanghao Li, Piotr Dollár, and Ross Girshick. Masked autoencoders are scalable vision learners. In *CVPR*, 2022.

[Ho *et al.*, 2020] Jonathan Ho, Ajay Jain, and Pieter Abbeel. Denoising diffusion probabilistic models. *NeurIPS*, 33, 2020.

[Huang *et al.*, 2021a] Jiahui Huang, Shi-Sheng Huang, Haoxuan Song, and Shi-Min Hu. Di-fusion: Online implicit 3d reconstruction with deep priors. In *CVPR*, 2021.

[Huang *et al.*, 2021b] Xiaohong Huang, Zhipang Deng, Dandan Li, and Xueguang Yuan. Missformer: An effective medical image segmentation transformer. *arXiv preprint arXiv:2109.07162*, 2021.

[Hui *et al.*, 2019] Zheng Hui, Xinbo Gao, Yunchu Yang, and Xiumei Wang. Lightweight image super-resolution with information multi-distillation network. In *MM*, 2019.

[Ioffe, 2015] Sergey Ioffe. Batch normalization: Accelerating deep network training by reducing internal covariate shift. *arXiv preprint arXiv:1502.03167*, 2015.

[Isensee *et al.*, 2021] Fabian Isensee, Paul F Jaeger, Simon AA Kohl, Jens Petersen, and Klaus H Maier-Hein. nnunet: a self-configuring method for deep learning-based biomedical image segmentation. *Nat Methods*, 18(2), 2021.

[Jha *et al.*, 2019] Debesh Jha, Pia H Smedsrød, Michael A Riegler, Dag Johansen, Thomas De Lange, Pål Halvorsen,

and Håvard D Johansen. Resunet++: An advanced architecture for medical image segmentation. In *ISM*. IEEE, 2019.

[Jing and Tian, 2020] Longlong Jing and Yingli Tian. Self-supervised visual feature learning with deep neural networks: A survey. *IEEE TPAMI*, 43(11), 2020.

[Kairouz and McMahan, 2021] Peter Kairouz and H Brendan McMahan. Advances and open problems in federated learning. *Found Trends Mach Learn*, 14(1-2), 2021.

[Kuriakose and others, 2023] B. M. Kuriakose et al. Edsr: Empowering super-resolution algorithms with high-quality div2k images. *Intell Decis Technol*, 17(4):1249–1263, 2023.

[Liang *et al.*, 2021] Jingyun Liang, Jie Zhang, Cao, Guolei Sun, Kai Zhang, Luc Van Gool, and Radu Timofte. Swinir: Image restoration using swin transformer. In *ICCV*, 2021.

[Lin and Chen, 2026] Zhen-Xin Lin and Shang-Kuan Chen. Phase4dfd: Multi-domain phase-aware attention for deepfake detection. *arXiv preprint arXiv:2601.05861*, 2026.

[Litjens *et al.*, 2017] Geert Litjens, Thijs Kooi, Babak Ehteshami Bejnordi, Arnaud Arindra Adiyoso Setio, Francesco Ciompi, Mohsen Ghafoorian, Jeroen Awm Van Der Laak, Bram Van Ginneken, and Clara I Sánchez. A survey on deep learning in medical image analysis. *Med Image Anal*, 42, 2017.

[Milletari *et al.*, 2016] Fausto Milletari, Nassir Navab, and Seyed-Ahmad Ahmadi. V-net: Fully convolutional neural networks for volumetric medical image segmentation. In *3DV*. IEEE, 2016.

[Oktay *et al.*, 2018] Ozan Oktay, Jo Schlemper, Loic Le Folgoc, Matthew Lee, Matthias Heinrich, Kazunari Misawa, Kensaku Mori, Steven McDonagh, Nils Y Hammerla, Bernhard Kainz, et al. Attention u-net: Learning where to look for the pancreas. *arXiv preprint arXiv:1804.03999*, 2018.

[Park *et al.*, 2003] S. C. Park, M. K. Park, and M. G. Kang. Super-resolution image reconstruction: a technical overview. *IEEE Signal Process. Mag.*, 20(3), 2003.

[Sun *et al.*, 2023] Long Sun, Jiangxin Dong, Jinhui Tang, and Jinshan Pan. Spatially-adaptive feature modulation for efficient image super-resolution. In *ICCV*, 2023.

[Tomczak and Welling, 2018] Jakub Tomczak and Max Welling. Vae with a vampprior. In *AISTATS*. PMLR, 2018.

[Vedaldi and Lenc, 2015] A. Vedaldi and K. Lenc. Matconvnet – convolutional neural networks for matlab. In *MM*, 2015.

[Wang *et al.*, 2018] Xintao Wang, Ke Yu, Shixiang Wu, Jin-jin Gu, Yihao Liu, Chao Dong, Yu Qiao, and Chen Change Loy. Esrgan: Enhanced super-resolution generative adversarial networks. In *ECCV Workshops*, 2018.

[Wang *et al.*, 2023] Hang Wang, Xuanhong Chen, Bingbing Ni, Yutian Liu, and Jinfan Liu. Omni aggregation networks for lightweight image super-resolution. In *CVPR*, 2023.

[Xiang *et al.*, 2023] Tiange Xiang, Mahmut Yurt, Ali B Syed, Kawin Setsompop, and Akshay Chaudhari. Ddm: Self-supervised diffusion mri denoising with generative diffusion models. *arXiv preprint arXiv:2302.03018*, 2023.

[Xie *et al.*, 2022] Zhenda Xie, Zheng Zhang, Yue Cao, Yutong Lin, Jianmin Bao, Zhuliang Yao, Qi Dai, and Han Hu. Simmim: A simple framework for masked image modeling. In *CVPR*, 2022.

[Xu *et al.*, 2019] Zhi-Qin John Xu, Yaoyu Zhang, Tao Luo, Yanyang Xiao, and Zheng Ma. Frequency principle: Fourier analysis sheds light on deep neural networks. *arXiv preprint arXiv:1901.06523*, 2019.

[Zamir *et al.*, 2022] Syed Waqas Zamir, Aditya Arora, Salman Khan, Munawar Hayat, Fahad Shahbaz Khan, and Ming-Hsuan Yang. Restormer: Efficient transformer for high-resolution image restoration. In *CVPR*, 2022.

[Zhang *et al.*, 2018] Kai Zhang, Wangmeng Zuo, and Lei Zhang. Ffdnet: Toward a fast and flexible solution for cnn-based image denoising. *IEEE TIP*, 27(9), 2018.

[Zhang, 2019] Richard Zhang. Making convolutional networks shift-invariant again. In *ICML*. PMLR, 2019.

[Zhou *et al.*, 2019] Zongwei Zhou, Vatsal Sodha, Md Mahfuzur Rahman Siddiquee, Ruibin Feng, Nima Tajbakhsh, Michael B Gotway, and Jianming Liang. Models genesis: Generic autodidactic models for 3d medical image analysis. In *MICCAI*. Springer, 2019.